Zhao et al. *Microsystems & Nanoengineering* (2025)11:82
https://doi.org/10.1038/s41378-025-00914-6

Microsystems & Nanoengineering
www.nature.com/micronano

ARTICLE Open Access

A programmable magnetic digital microfluidic platform integrated with electrochemical detection system

Yong Zhao[1,2], Shuyue Jiang[1,3], Gaozhe Cai[4]✉, Lihua Wang[5]✉, Jianlong Zhao[1,6] and Shilun Feng[1]✉

Abstract

Digital microfluidic (DMF) technology is widely used in bioanalysis and chemical reactions due to its accuracy and flexibility in manipulating droplets. However, most DMF systems usually rely on complex electrode fabrication and high driving voltages. Sensor integration in DMF systems is also quite rare. In this study, a programmable magnetic digital microfluidic (PMDMF) platform integrated with electrochemical detection system was proposed. It enables non-contact, flexible droplet manipulation without complex processes and high voltages, meeting the requirements of automated electrochemical detection. The platform includes a magnetic control system, a microfluidic chip, and an electrochemical detection system. The magnetic control system consists of a microcoil array circuit board, a N52 permanent magnet, and an Arduino control module. N52 magnets generate localized magnetic fields to drive droplet movement, while the Arduino module enables programmable control for precise manipulation. The maximum average velocity of the droplet is about 3.9 cm/s. The microfluidic chip was fabricated using 3D printing and the superhydrophobic surface of chip was fabricated by spray coating. The electrochemical detection system consists of the MoS_2@CeO_2/PVA working electrode, Ag/AgCl reference electrode, and carbon counter electrode. To evaluate the practical value of the integrated platform, glucose in sweat was automatically and accurately detected. The proposed platform has a wide linear detection range (0.01–0.25 mM), a lower LOD (6.5 μM), a superior sensitivity (7833.54 μA·mM^{-1}·cm^{-2}), and excellent recovery rate (88.1–113.5%). It has an extensive potential for future application in the fields of medical diagnostics and point-of-care testing.

Introduction

Conventional continuous-flow microfluidic systems have demonstrated great capability in handling liquid with the small volume. These systems usually require microchannel structures and pumping systems[1,2], which limit their integration and scalability. To overcome these limitations, digital microfluidic (DMF) technology has attracted much attention[3]. For the DMF technology, various methods have been explored to precisely control the position and behavior of droplet. These methods include electric fields[4–7], magnetic fields[8–10], acoustic waves[11], optical fields[12], and others. For example, DMFs based on electrowetting-on-dielectric (EWOD) can allow manipulate droplets by generating localized electric fields at the electrodes, thus avoiding the need for microchannel structures and external pumps. This allows it to exhibit unique advantages in the precise manipulation of tiny droplets, complex droplet manipulation, and multi-step reaction processes[13–15]. However, these DMF techniques, which rely on complex electrode fabrication and high driving voltages[13,16], restrict the processing of certain biological samples and reduce the stability and reliability of the system.

Correspondence: Gaozhe Cai (caigaozhe@shu.edu.cn) or
Lihua Wang (wanglihua@shu.edu.cn) or
Shilun Feng (shilun.feng@mail.sim.ac.cn)
[1]State Key Laboratory of Transducer Technology, Shanghai Institute of Microsystem and Information Technology, Chinese Academy of Sciences, Shanghai 200050, China
[2]School of Graduate Study, University of Chinese Academy of Sciences, Beijing 100049, China
Full list of author information is available at the end of the article
These authors contributed equally: Yong Zhao, Shuyue Jiang.

Magnetic digital microfluidics offers a new approach. Although removing the electrodes may affect droplet splitting, the unique advantages of magnetic droplet actuation remain significant. The distinctive features of magnetic digital microfluidics include the actuation of magnetic particles(MNPs), simple fabrication, no high voltage driving requirements and flexible manipulation. Although the track of droplet can be programmed on an EWOD platform, it must follow predefined electrode paths and lack of flexibility. In contrast, magnetic digital microfluidic platform enable contactless droplet manipulation without requiring electrode patterns design[17]. The transport path of droplet is programmable and can be reconfigured according to specific needs. This technique uses an external magnetic system to control the generation of a localized magnetic field by permanent magnets[18–20] or an electromagnet[21–25]. Droplet actuation requires the magnetic field to control either the magnetic particles within the droplet or the magnetic material surrounding it[26,27]. Huang et al. developed a microfluidic system based on droplet arrays for chemiluminescence immunoassay of procalcitonin[20]. By moving permanent magnets through a stepper motor, magnetic beads can be aggregated, released, transferred and mixed between droplets. Saroj et al. achieved efficient mixing of two solutions in a microlitre droplet by adjusting the current and frequency of four sets of energized coils[25]. The static magnetic field driving mode is simple to operate, but typically requires bulky displacement control platforms for permanent magnets, which hinders integration. Alternatively, the electromagnetic field driving mode manipulates droplets through the dynamic magnetic field generated by energized coils.Coils fabricated on PCB are more conducive to integration, but the magnetic field strength produced under low currents is often insufficient. Increasing the current can enhance the magnetic field, but the associated heat generated by the excessive coil currents may interfere with biological detection.Therefore, it is crucial to develop an efficient and easily integrated droplet manipulation technique by combining the advantages of static magnetic and electromagnetic fields.

Furthermore, sensor integration in DMF systems is quite rare. Most of digital microfluidic or magnetic digital microfluidic integrated detection platforms are based on optical detection, such as fluorescence detection[28–30], chemiluminescence[31], and colorimetric sensing[32,33]. The application of these methods in portable devices in the field is limited due to the complexity of optical detection devices[13]. Among the many detection methods, electrochemical detection is ideal for combining with microfluidic platforms due to its simplicity, low cost, high sensitivity, and integrability[34–36]. The main detection component of an electrochemical device is the electrode, which can be miniaturized, batch-fabricated, and multiplexed[37,38]. By combining magnetic digital microfluidics with electrochemical detection, sample manipulation can be performed on the chip and provide automated detection. This enables integrated and automated analytical processes, further expanding the application of magnetic digital microfluidic platforms in the field of automated detection[39].

In this work, we propose a novel programmable magnetic digital microfluidic platform that automates the control of droplet transportation and real-time continuous electrochemical detection. The PMDMF platform includes a magnetic control system, a microfluidic chip, and an electrochemical detection module. The magnetic control system consists of a microcoil array printed circuit board (PCB), a N52 permanent magnet, and an Arduino control module. The combination of microcoils (2.737 mm) and a millimeter-scale cylindrical magnet (4 mm) greatly reduces the size of the device and improves the integration. The Arduino controls the specific coils to generate an induced magnetic field to drive the N52 permanent magnet. The magnet is responsible for generating a localized high-intensity magnetic field to actuate the magnetic droplets. For continuous detection of multiple samples, the microfluidic chip is set up with five sample wells. It was fabricated by 3D printing, avoiding the complicated photolithography and PDMS preparation process. In order to reduce resistance for droplet manipulation, the chip surface was sprayed with a superhydrophobic coating. The droplet's movement trajectory is programmable and can be flexibly adjusted based on specific requirements. To facilitate the integration with the microfluidic chip and highly sensitive detection, the detection electrode is fabricated by PCB process, and the working electrode is based on MoS_2@-CeO_2/PVA. The platform can be used for droplet manipulation and highly sensitive electrochemical detection of targets, and its effectiveness has been validated in the practical detection of glucose in PBS and sweat.

Materials and methods

Materials

N52 permanent magnet was purchased from Shenzhen LaLa Magnetic Material Development Co., Ltd. Magnet nanoparticles solution (Fe_3O_4) was obtained from Shanghai Macklin Biochemical Technology Co., Ltd. The superhydrophobic coating reagent NC306 was purchased from Changzhou Nakeluo New Material Technology Co., Ltd. 207 C and 204S were purchased from Dongguan Zhongke Leader Technology Co., Ltd. Conductive silver paste and conductive carbon paste were purchased from Shenzhen Sien Screen Printing Material Co., Ltd. Polyvinyl alcohol (PVA) was purchased from Shanghai Zhan Yun Chemical Co., Ltd. Artificial sweat (PH8.0) was purchased from Shanghai Yuanye Biotechnology Co., Ltd.

Other PBS buffer, glucose, MoS_2, and CeO_2 reagents were purchased from Shanghai Titan Technology Co., Ltd.

Programmable magnetic control system

The magnetic control system consists of a microcoil array circuit board, a permanent magnet (NdFeB N52, 4 × 2 mm), and an Arduino UNO controller module. The coil array circuit consists of CD74HC4067, ULN2803, NMOS, PMOS, diodes, and microcoil parts (2.737 × 2.737 mm). The microcoil is formed through PCB trace routing, and the circuit is designed by Jialichuang EDA. The PCB is processed by Hangzhou Jiepei Information Technology Co., Ltd. The coil current is supplied by a DC power(UNI-T, UTP1306S). Arduino can easily and efficiently control the on/off of the coil in the magnetic control system, and the N52 permanent magnet can be operated to move on its surface after writing continuous commands. Two types of PCBs: a 10 × 10 coil array PCB with dimensions 84 × 52 mm and a 32 × 24 coil array PCB with dimensions 170 × 100 mm were designed. The induced magnetic fields of the coil with different currents were measured using a handheld digital Tesla meter (KT-102, ±2%), and the coil ($z = 0$ mm) temperature was measured using a contact thermometer (DT1310).

Magnetic field simulation

To compare the effects of coil layers and structure on the magnetic field and to understand the strong magnetic field of the magnet, magnetic field simulations were conducted using COMSOL Multiphysics. The coil material is copper with a conductivity of 5.998e7 (S/m), and the size is 2.737 × 2.737 mm. The magnet material is NdFeB (N52,4 × 2 mm), and the surrounding domain is air. Steady state solutions are performed using the magnetic field (mf) and magnetic field no current (mfnc) physical fields.

Microfluidic chip fabrication

For simplicity and convenience, the microfluidic chip was designed using SOLIDWORKS and fabricated through 3D printing (Form3 + , Formlabs). The dimensions are 72.5 × 51.3 mm. The chip surface was made superhydrophobic by spraying 204S reagent. Contact angle measurement was assisted by a contact angle meter (Attension Theta Flex, Biolin Scientific), and ImageJ software.

Preparation of electrochemical detection system

The electrochemical detection system includes multiple sensing electrodes. The electrodes designed by Jialichuang EDA has a size of 11 × 9 mm and working electrode area of 0.00817 cm^2, as shown in Fig. S7. The electrode was processed by Hangzhou Express Electronics Co., Ltd. The working electrode is coated with MoS_2@CeO_2/PVA hydrogel, the reference electrode is coated with silver paste, and the counter electrode is coated with carbon paste. The reproducibility, repeatability, and stability of the glucose sensor have been added in the supplementary material (Fig. S8).

Integration of PMDMF platform

The magnetic control system is connected to the DC power supply and the Arduino controller. The electrochemical detection system and microfluidic chip were glued together to ensure that they were level. Place it 3.8 mm above the surface of the coil.

Preparation of MoS_2@CeO_2/PVA hydrogels

2 g of polyvinyl alcohol (PVA) was dissolved in 30 mL of water with heating and stirring to obtain PVA hydrogel. 0.2 g CeO_2 nanoparticles were dispersed 5 mL in ethanol solution, and then 0.2 g MoS_2 nanoparticles were added under constant magnetic stirring to obtain MoS_2@CeO_2 dispersion. Finally, the MoS_2@CeO_2 dispersion was redispersed in a PVA hydrogel with heating and stirring to obtain a homogeneous MoS_2@CeO_2/PVA hydrogel.

Droplet Manipulation

The velocity of the magnet's movement can be adjusted by changing the time interval between coil activations, which in turn alters the droplet transportation velocity. The maximum droplet velocity is determined when the magnet's movement velocity increases to the point where the droplet can no longer stably follow. Record the motion video using CCD camera and import it into tracker software to analyze the motion process.During the experiment, in order to quantify the mixing effect, the microfluidic area was video recorded and the corresponding video frames were imported into Matlab (Mathworks). The mixing index was calculated by image analysis by identifying the boundaries of the droplets at the software level.

Application of the PMDMF platform to electrochemical detection

First, glucose in PBS buffer was tested to verify the electrochemical properties. After obtaining the linear regression equation of peak current and glucose concentration, glucose in artificial sweat was further detected. Recovery experiments were carried out using the standard addition method by adding glucose with the standard concentration of 0.05, 0.1, 0.15, 0.2 and 0.25 mM. Finally, the measured values and recoveries were calculated.

Results and discussion

Design of PMDMF platform

Unlike most previously reported magnetic manipulation systems[20–22], the proposed magnetic manipulation system

is a combination of a microcoil array and a millimeter-scale magnet, with individual square coils of size 2.737 mm, cylindrical magnets of diameter 4 mm in Fig. 1a. Coils are spaced 0.1 mm apart, only part of the array is shown here for clarity. The microcoil array is responsible for driving the precise movement of the magnet above it. A 32 × 24 coil array was designed to meet the needs of the scale of movement required by the magnet during the detection process. This design can greatly reduce the size of the magnetic control system and improves integration. In addition, there is no need for predefined electrode patterns as in EWOD[13]. A microfluidic chip integrated with electrochemical detection system is shown in Fig. 1b. Conventional fabrication methods of microfluidic chips, such as photolithography and soft lithography, usually require expensive equipment and rely on strict cleanroom conditions. For flexibility and low cost, the microfluidic chip was fabricated using 3D printing. As shown in Fig. 1c, the side view of the PMDMF platform is composed of an electromagnetic coils layer, a magnet layer, a microfluidic and an electrochemical sensing layer from bottom to top. The microfluidic surface is a superhydrophobic coating to reduce the movement resistance of droplets. The droplets in the chip are actuated by a magnet with strong magnetic properties underneath. Multiple electrochemical detection electrodes were fabricated and adhered to the sides of the microfluidic chip. The detection electrodes were at the same level as the microfluidic chip. Figure 1d shows the detailed structure of the PMDMF platform. The magnetic control system, microfluidic chip and electrochemical detection system are assembled together. Following the design of the droplet movement path, the magnetic control system autonomously drives multiple sample droplets in succession to the detection electrode for analysis. The working electrode here is based on MoS_2@CeO_2/PVA hydrogel, which improves the performance of the electrode and enhances the sensitivity of the detection. Its preparation process is shown in Fig. S1. To validate the functionality of the platform, the glucose in the sweat are detected by DPV technology and the results curves display on the computer screen.

The principle and simulation of the magnetic control system

While EWOD system focuses on electrical drives, the magnetic digital microfluidics focuses on magnetic drives. In the magnetic control system, the movement of the

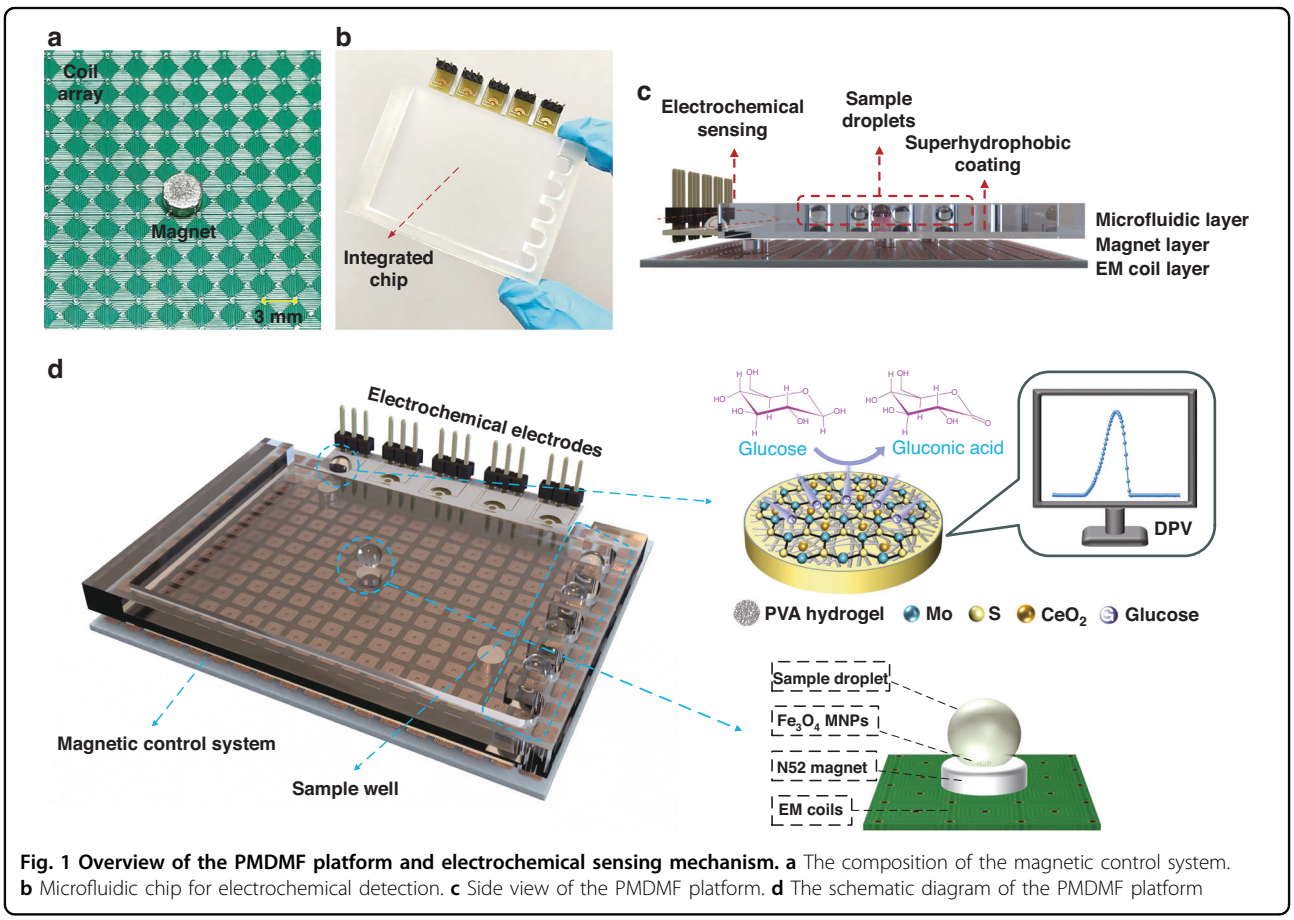

Fig. 1 Overview of the PMDMF platform and electrochemical sensing mechanism. a The composition of the magnetic control system. **b** Microfluidic chip for electrochemical detection. **c** Side view of the PMDMF platform. **d** The schematic diagram of the PMDMF platform

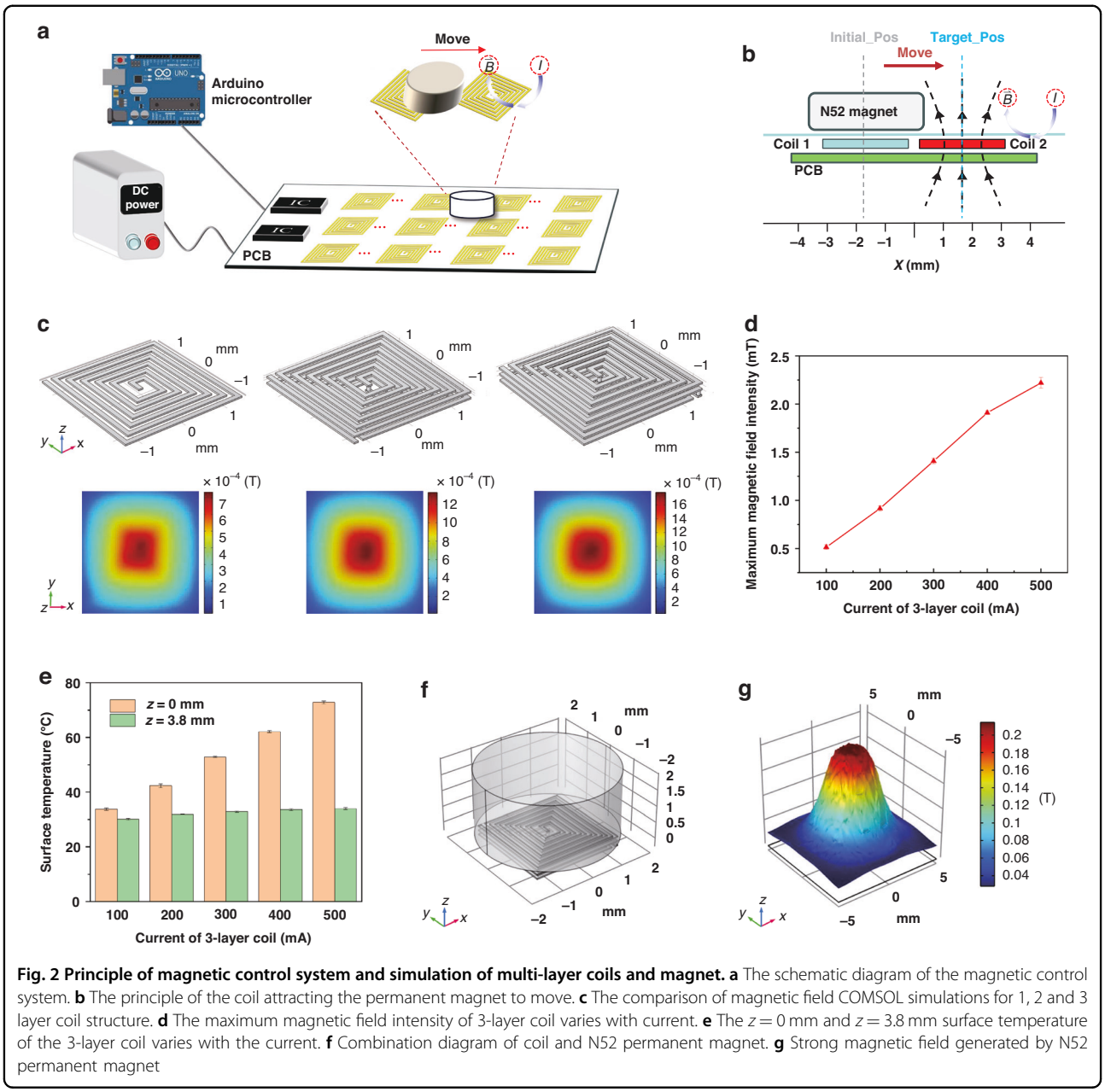

Fig. 2 Principle of magnetic control system and simulation of multi-layer coils and magnet. a The schematic diagram of the magnetic control system. **b** The principle of the coil attracting the permanent magnet to move. **c** The comparison of magnetic field COMSOL simulations for 1, 2 and 3 layer coil structure. **d** The maximum magnetic field intensity of 3-layer coil varies with current. **e** The $z = 0$ mm and $z = 3.8$ mm surface temperature of the 3-layer coil varies with the current. **f** Combination diagram of coil and N52 permanent magnet. **g** Strong magnetic field generated by N52 permanent magnet

magnet determines whether the magnetic droplets can be actuated precisely or not. In order to program a specific coil, the coil circuit is considered to be fabricated on a PCB board (Fig. 2a). When an adjacent coil is turned on, an induced magnetic field is generated around that coil according to Ampere's law. When the magnetic field is large enough, the magnet will move to the position of the turned-on coil under magnetic attraction. As Fig. 2b illustrates, coil1 on the PCB is turned off with no magnetic field, and coil2 is turned on to generate an induced magnetic field. According to the right-handed helix rule, the direction of the induced magnetic field can be determined, and the N52 magnet will move from the Intial_Pos to the Target_Pos. When the microcontroller is programmed to write the switching sequence, the coil generates an induced magnetic field in sequence. Then, the magnet is attracted to move along the set route. To evaluate the influence of induced magnetic fields generated by electromagnetic coils of varying layers, magnetic field simulations were conducted for coils with 1, 2, and 3 layers. As shown in the magnetic field cloud diagram (Fig. 2c), it is evident that the center of the 3-layer magnetic field uniformity is the best and the magnetic field strength is the largest. Therefore, the 3-layer coil structure was chosen for the magnetic system. According to the law of Ampere, the current is proportional to the magnetic field

strength of the coil, which is also shown in Fig. 2d. When current flows through the coil, it generates heat on the surface. If the current is too high, it may exceed the carrying capacity of the PCB chip and potentially interfere with the biological detection process. For this reason, temperatures were measured at the $z = 0$ mm surface of the coil and at the $z = 3.8$ mm (microfluidic chip location) surface. The initial temperature in the chamber was 29.3 °C (summer), and as the results in Fig. 2e, the temperature of the $z = 0$ mm surface basically increases proportionally with the current, and the temperature of the $z = 3.8$ mm surface is almost unaffected. This indicates that the heat generated by the coil does not cause any temperature variation in the microfluidic chip. Furthermore, since the actual energization time of the coil is on the millisecond scale, its impact is even more negligible. Combining the actual magnet testing with the temperature results, 300 mA is the suitable coil current and can generate a magnetic field strength of about 1 mT. As shown in Fig. 2f and g, the simulation results show that the N52 permanent magnet can generate a high-intensity magnetic field of about 200 mT. Therefore, it is considered that the actuation of the droplet is all from the action of the permanent magnet.

Magnetic droplet manipulation

To investigate the manipulation ability of the proposed magnetic control system, the movement and force states of droplet on the microfluidic chip were analyzed. As indicated by Fig. 3a and tested in Fig. S2, the droplet cannot move on the untreated surface under the drive of magnetic field, owing to the larger resistance force between droplet and substrate. To reduce the resistance force, The chip surface was fabricated to the superhydrophobic state by spraying coating. In Fig. 3b, various hydrophobic reagents were evaluated through contact angle measurements. The 204S hydrophobic reagent has the best effect with a contact angle of 158.4°. Therefore, droplet can be manipulated when magnet is used and the substrate surface is superhydrophobic. On the superhydrophobic surface, a magnetic droplet is dominated by three main forces: the magnetic force F_m, the friction between the droplet and the substrate F_f, and the capillary force generated by the deformation of the droplet F_c (Fig. S3). During the movement of the droplet, the magnetic particles inside are subjected to the magnetic force of the magnet below[24,40], which can be expressed as:

$$F_m = \frac{V\chi}{\mu_0(1+\chi)}(B \cdot \nabla)B \tag{1}$$

where V is the volume of the magnetic droplet, χ is the magnetic susceptibility of the magnetic particles, μ_0 is the permeability of vacuum, and B is the magnetic field strength applied to the droplet by the N52 permanent magnet. In addition to the magnetic force, the droplet motion is also subject to a friction force with the substrate, which can be expressed as:

$$F_f = k(mg + F_{my}) \tag{2}$$

where k is the coefficient of friction between the droplet and the substrate, m is the mass of the droplet, g is the acceleration of gravity, and F_{my} is the vertical component of the magnetic force. In addition, the magnetic droplet motion produces a deformation that generates a capillary force against the motion[41], which can be expressed as:

$$F_c \approx 2\gamma R(cos\theta_A - cos\theta_R) \tag{3}$$

where γ is the surface tension of the droplet, R represents the contact line radius of the droplet, θ_A is the advancing contact angle, and θ_R is the receding contact angle. In summary, the kinetic behavior of the droplet on the platform can be described as $F_m - F_f - F_c = ma$. On a superhydrophobic surface, the droplet deformation is typically small, resulting in relatively weak capillary force (Fig. 3ci). The movement of the magnetic droplet is primarily driven by magnetic forces, which are determined by the concentration of magnetic particles within the droplet, the magnetic field strength of the magnet, and the distance between the droplet and the magnet. As illustrated in Fig. 3cii, the program-controlled droplet motion can depict various letters such as “S”, “I”, “M”, “I”and “T”, demonstrating the platform’s flexible control capabilities (Video S1).

We calculated the maximum average velocity of droplets with different volumes under magnetic actuation (Fig. 3d). Small droplets (<5 μL) have lower inertia, requiring less driving force to move. The magnetic particles act more evenly in the droplets, and the droplet shape remains stable during movement. Therefore, under the action of the magnetic field, the droplets can accelerate and tend to a stable maximum speed. As the droplet volume increases, the droplet inertia and the friction between the droplet and the substrate increase. The magnetic particles may not be able to transmit the driving force uniformly, resulting in dragging of localized areas of the droplet. In this case, maintaining the motion of the droplet in a stable shape will reduce the speed. When the droplet volume increases to a certain extent, the magnetic response is no longer sufficient to drive larger droplets. The maximum droplet volumes driven by 0.25 μL MNPs, 0.5 μL MNPs, 1.0 μL MNPs, 1.5 μL MNPs, and 2.0 μL MNPs are 50 μL, 80 μL, 100 μL, 150 μL, and 220 μL, respectively. In addition, for the same volume of droplets, more MNPs loading increases the magnetic response intensity of the droplets, resulting in higher speeds.The maximum droplet movement velocity is about 3.9 cm/s

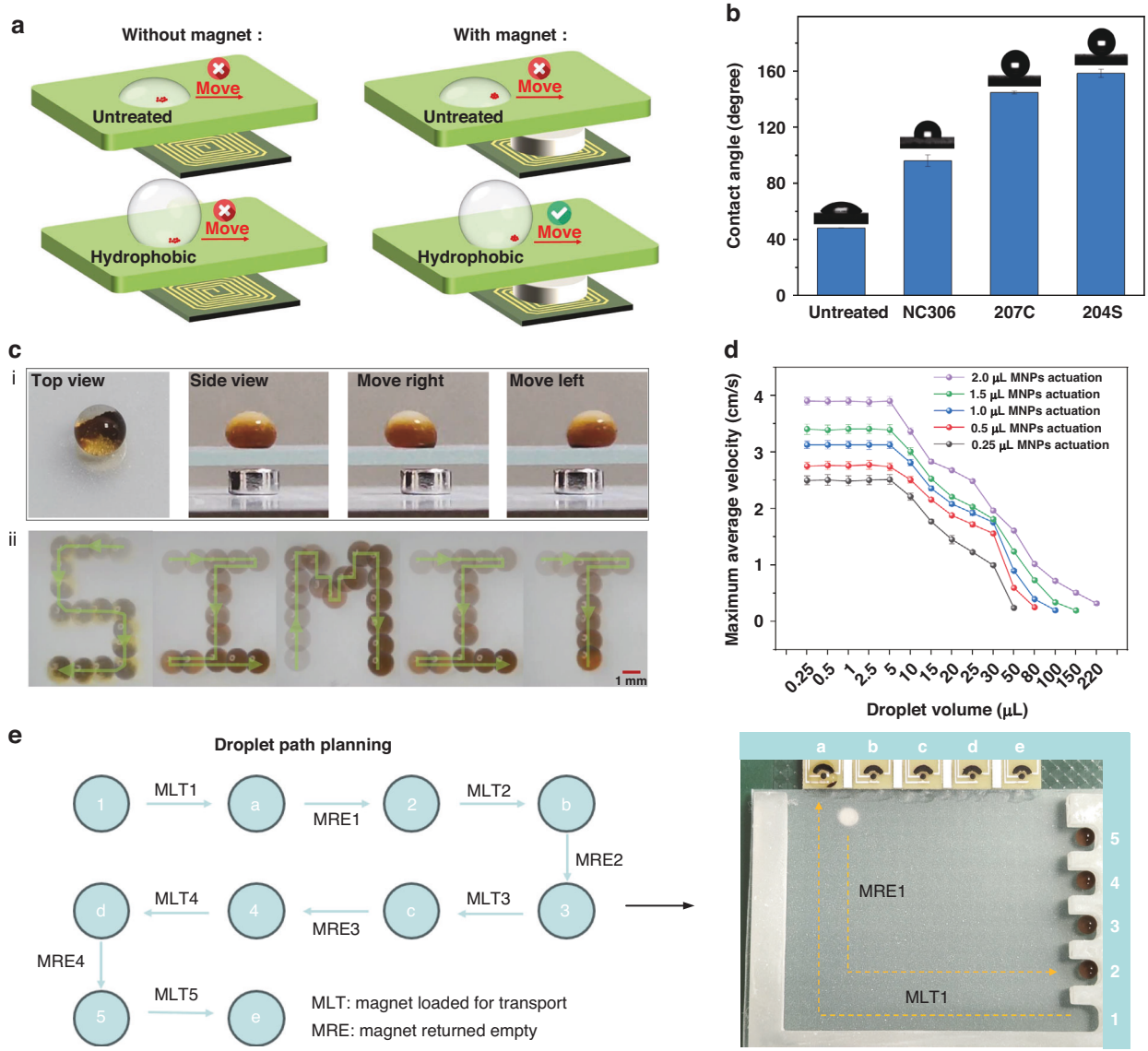

Fig. 3 Characterization of magnetic droplet manipulation and demonstration of continuous electrochemical detection of multiple droplets. a Comparison of droplet magnetic actuation methods. **b** Hydrophobic properties of different reagents. **c** Snapshots of droplet motion. **cii** Video frame overlay of droplet motion paths: "S, I, M, I, T". **d** Maximum average velocity at different magnetic droplet concentrations and volumes. **e** Schematic diagram of the continuous transportation of droplets to the detection zone

(5 V, 0.3 A), which is higher than the droplet velocities reported in many conventional EWOD systems and magnetically actuated systems[9,23]. For example, Jang et al. reported a droplet movement velocity of 0.7 cm/s (60 V) in an EWOD system (square electrode)[42], while Kremers et al.'s system (gold interdigitated electrode) was 3.3 cm/s (250 V)[43]. Figure S4 shows the mixing process of droplet. When the two droplets were close, they merged together. The movement of the MPs inside the droplets was driven by periodic movement of the magnet over short distances, thus promoting droplet mixing. Experimental results show that active mixing accelerates the mixing process inside the droplets through the periodic movement of the magnet, and is superior to non-active mixing in both mixing rate and final mixing degree. When the chip needs complex manipulation (splitting), surface energy trap (SET) processing is required. SET regulates surface energy to influence droplet contact line dynamics, creating preferential breakage points that enable controlled splitting[44] (Fig. S5). For the next application of electrochemical detection, Fig. 3e shows the setup of the droplet movement paths. The magnet loads droplet #1 and transports it to the a-electrode area. While detecting droplet #1, the magnet returns to load droplet #2 and transports it to the

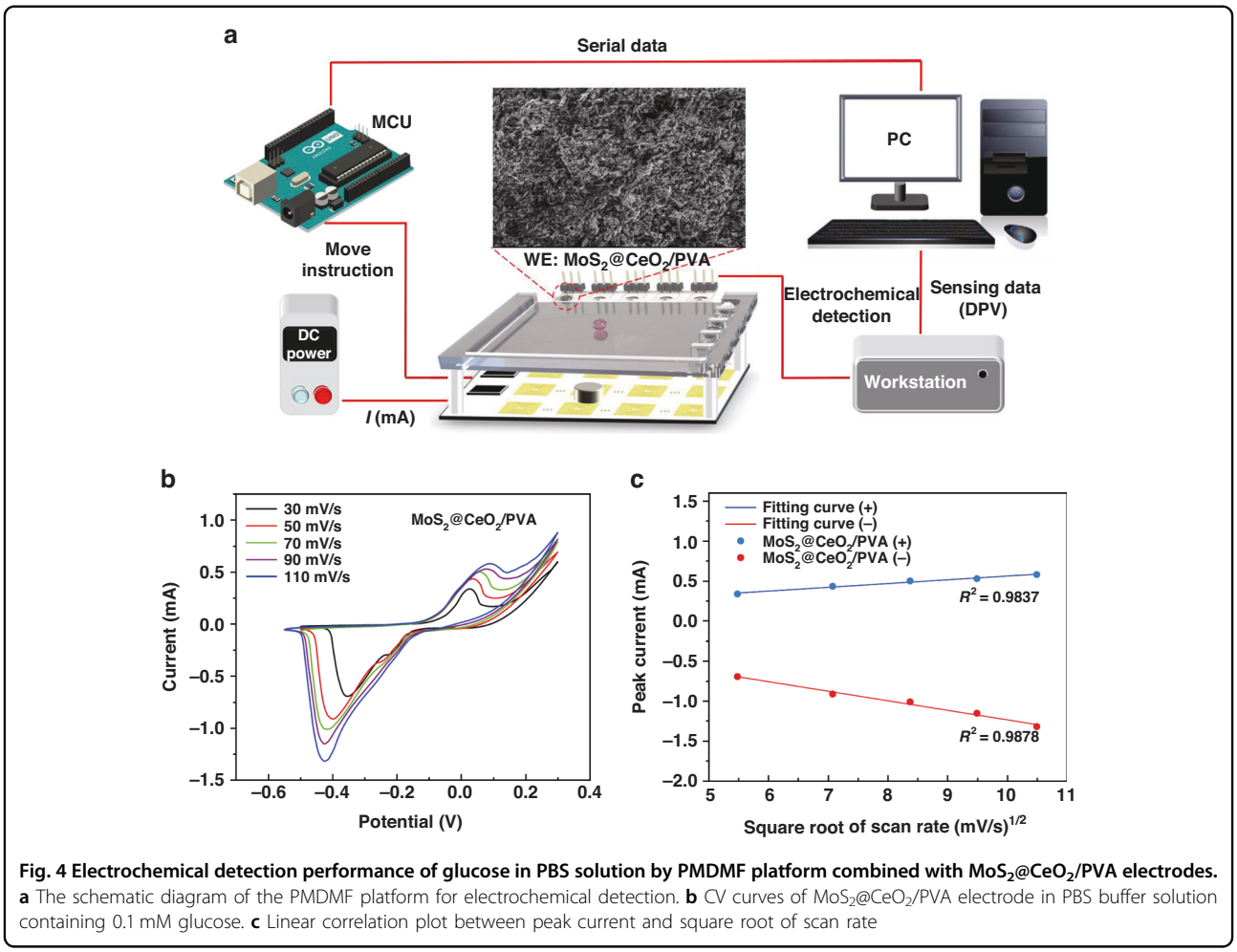

Fig. 4 Electrochemical detection performance of glucose in PBS solution by PMDMF platform combined with MoS_2@CeO_2/PVA electrodes. **a** The schematic diagram of the PMDMF platform for electrochemical detection. **b** CV curves of MoS_2@CeO_2/PVA electrode in PBS buffer solution containing 0.1 mM glucose. **c** Linear correlation plot between peak current and square root of scan rate

b-electrode area. This process continues until droplet #5 reaches the e-electrode area, enabling continuous detection of multiple samples.

Application of the PMDMF platform to electrochemical detection

Electrochemical properties of the PMDMF platform

To evaluate the practical value of the integrated platform, glucose in sweat was automatically and accurately detected. Figure 4a provides the schematic diagram of the PMDMF platform for electrochemical detection. An external DC power supply current to the PCB, while the Arduino is programmed to control the droplet's movement. The detection property of working electrode determines the accuracy and reliability of the whole signal. Therefore, the MoS_2@CeO_2/PVA composite was selected as the modification material for the working electrode. The SEM images of MoS_2@CeO_2/PVA reveal a three-dimensional layered structure with a high surface area, which provides numerous active sites for electrochemical reactions. To assess the effectiveness of the electrochemical detection on the platform, glucose was analyzed. Cyclic voltammetry (CV) can be used to analyze the redox potentials of substances and the kinetics of electrochemical reactions. In Fig. 4b, the CV electrochemical detection process was performed in PBS buffer containing 0.1 mM glucose at different scan rates. With the increase in scan rate, both the oxidation and reduction peaks rise, and the peak current shows a linear relationship with the square root of scan rate (Fig. 4c). When the scan rate is 50 mV/s, the anodic peak current is 0.7543 mA. These observations indicate that the MoS_2@CeO_2/PVA electrode exhibits strong redox capabilities towards glucose in PBS solution.

Glucose sensing performance of PMDMF platform

Compared with CV, differential pulse voltammetry (DPV) applies a pulsed voltage to the electrode to measure the current response. By reducing background current and enhancing the resolution of peak current signals, DPV serves as an effective analytical tool for glucose detection. The magnetic particles used in the current platform do

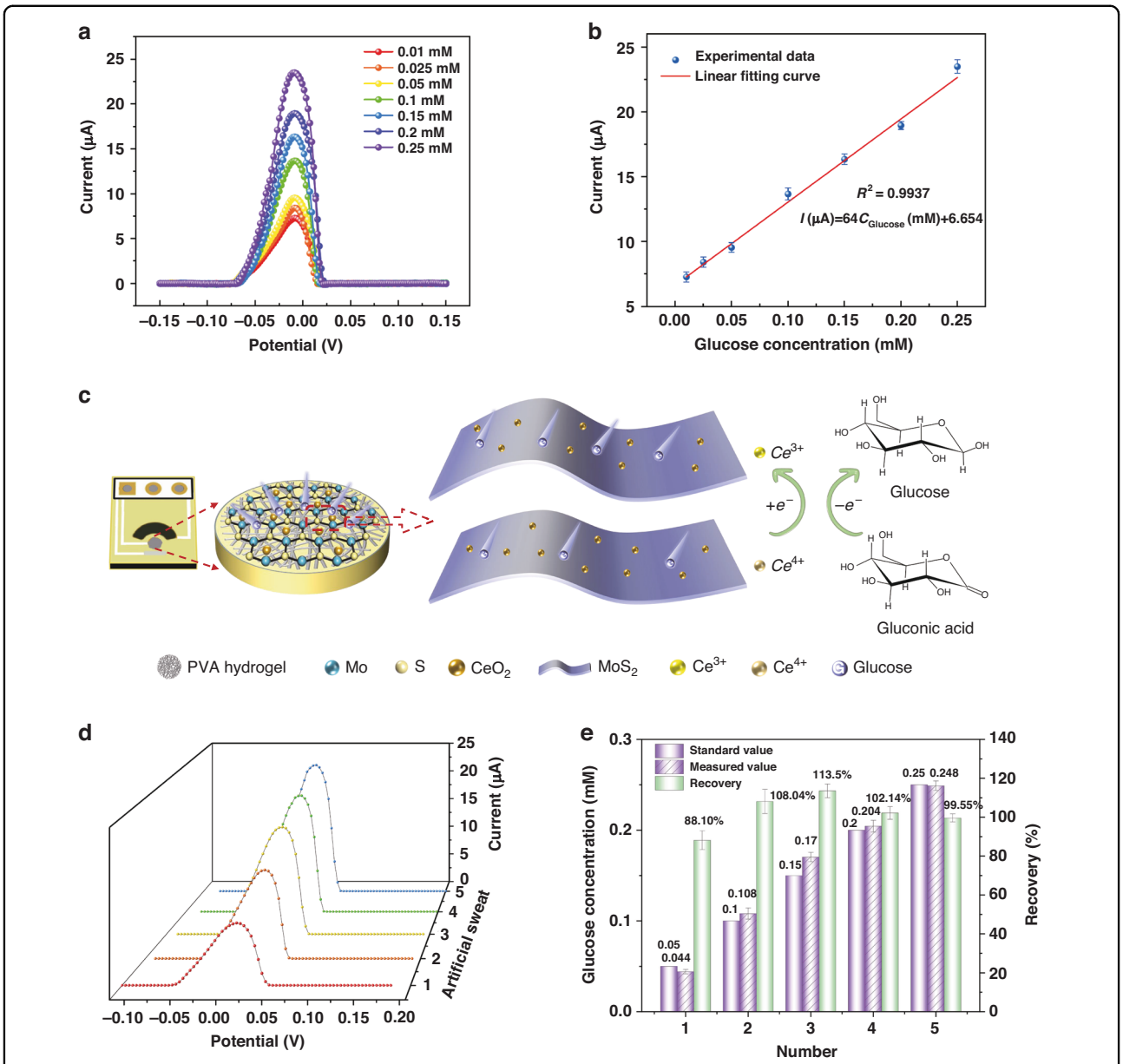

Fig. 5 Glucose sensing and recovery analysis of actual sweat samples by PMDMF platform. a DPV curves of droplets with different glucose concentrations at the electrode. **b** Linear correlation plot between glucose concentration and DPV response current. **c** Schematic diagram of the mechanism of glucose detection by MoS_2@CeO_2/PVA electrode. **d** DPV curves for five artificial sweat samples. **e** Glucose assay and recovery analysis of sweat samples

not interfere with the electrochemical detection of glucose (Fig. S6). The DPV response curve exhibits a distinct anodic peak, with the peak current gradually increasing as the glucose concentration rises (Fig. 5a). This indicates that the electrode material exhibits a good response to the redox reaction of glucose. As depicted in Fig. 5b, the results reveal a strong linear relationship between the DPV peak current and glucose concentration, with a correlation coefficient R^2 of 0.9937, which is close to 1. The linear regression equation can be expressed as $I\ (\mu A) = 64C_{Glucose}\ (mM) + 6.654$. Based on the linear fitting results, the sensitivity is determined by the slope of the curve and the area of the working electrode (0.00817 cm^2), thus the sensitivity of the sensor is 7833.54 ($\mu A \cdot mM^{-1} \cdot cm^{-2}$). The limit of detection (LOD) of the sensor can be calculated using the following formula: $LOD = 3\sigma/\alpha$, where σ is the standard deviation of the sensor and α is the slope of the linear regression curve shown in Fig. 5b. In this experiment, the standard deviation of $\sigma = 0.139\ \mu A$ was obtained from

Table 1 Comparison with the performance of electrochemical glucose sensors based on MoS_2 and other materials

Electrode material	Linear range (mM)	LOD (μM)	Sensitivity(μA·mM^{-1}·cm^{-2})	Ref
GCE/CNT/ MoS_2/NiNPs	0.05–0.65	0.2	1212	[46]
MoS_2@$CuCo_2O_4$	0.0005–0.393	0.5	1303	[47]
Pt/MXene/CH/Pt	0–8	29.15	3.43	[48]
CuS/MoS_2	0.1–11	1.52	252.71	[49]
MoS_2@AuNP	0.001–0.1	0.14	103.2	[50]
MoS_2@CeO_2/PVA	0.01–0.25	6.5	7833.54	This work

CNT carbon nanotube, *CH* conductive hydrogel

measurements of blank samples. Therefore, the limit of detection (LOD) of the sensor was calculated to be 6.5 μM. Figure 5c illustrates the glucose sensing mechanism of the MoS_2@CeO_2/PVA electrode. The CeO_2 distributed on the MoS_2 surface can adsorb and detect abundant glucose molecules through redox reactions. During the reaction process, CeO_2 undergoes redox cycling between Ce^{3+} and Ce^{4+}, facilitating electron transfer[45]. Glucose loses electrons at the electrode surface and is oxidized to gluconic acid. The flow of electrons generated during the electrochemical reaction produces a current signal. To better validate the usefulness of the detection platform, it is important to detect glucose levels in sweat. All experiments used artificial sweat with a pH of 8.0. Standard glucose solutions with concentrations of 0.05, 0.1, 0.15, 0.2, and 0.25 mM were added to the sweat samples for recovery experiments. Using the droplet transportation path described in Fig. 3e, continuous electrochemical detection of five sweat samples with different concentrations was performed. As shown in Fig. 5d, the DPV curves exhibit anodic peaks similar to those in PBS buffer solution, indicating consistent electrochemical behavior of the detection platform in sweat. The results shown in Fig. 5e demonstrate that the detection platform achieved excellent recovery rates ranging from 88.1% to 113.5%. These results suggest that the platform can be used for glucose concentration detection in sweat.

Table 1 compares the performance of MoS_2@CeO_2/PVA electrode with other sensing electrodes for glucose detection. The results show that the MoS_2@CeO_2/PVA electrode has a linear detection range of 0.01–0.25 mM and a limit of detection (LOD) of 6.5 μM. It also exhibits the highest sensitivity (7833.54 μA·mM^{-1}·cm^{-2}), which is much better than that of the comparable MoS_2-based electrodes such as MoS_2@CuC_2O_4 (1303 μA·mM^{-1}·cm^{-2}) and MoS_2@AuNP (103.2 μA·mM^{-1}·cm^{-2}). The excellent performance of the electrode is attributed to the synergistic interaction between MoS_2 and CeO_2. MoS_2 provides abundant active sites, while CeO_2 has excellent redox capacity, thus enhancing the electrocatalytic efficiency of the glucose oxidation reaction. In addition, the PVA hydrogel improves the mechanical stability of the electrode and enhances the ion transport ability. Therefore, the electrode exhibits significant advantages in glucose detection applications.

Conclusions

In summary, we developed a programmable magnetic digital microfluidic platform integrated with electrochemical detection system and applied it to glucose detection in artificial sweat. Firstly, the optimal number of coil layers in the magnetic control system was determined through COMSOL simulations. Considering the magnetic field effectiveness, heat generation, and actual testing results, a 3-layer coil structure with a current of 300 mA was selected. The magnetic control system generates a localized high-intensity magnetic field through the movement of N52 permanent magnets. The coil array operates without the need for high-voltage drive (5 V, 0.3 A), and its manufacturing process is simple, allowing for long-term reusability. Then, droplet manipulation on a superhydrophobic surface was studied, with the 204S hydrophobic reagent showing minimal resistance to droplet movement. The droplets can be manipulated to follow letter-shaped paths with a maximum average velocity of about 3.9 cm/s. The magnetic actuation method enables faster droplet movement and can carry larger droplet volumes. Finally, This platform realizes automated and continuous multiple single-sample electrochemical detection. The electrochemical detection electrodes consist of the MoS_2@CeO_2/PVA working electrode, Ag/AgCl reference electrode, and carbon counter electrode. The PMDMF platform demonstrated excellent glucose detection performance with a lower LOD(6.5 μM) and superior sensitivity (7833.54 μA·mM^{-1}·cm^{-2}). The recovery rate for glucose detection in artificial sweat ranged from 88.1% to 113.5%. The results exhibited the practicality of the integration platform in droplet manipulation and electrochemical detection. In the future, it is necessary to optimize hardware and algorithms to support

parallel operation of multiple droplets and explore the surface modification of MNPs to enhance compatibility with various biological samples.

Acknowledgements
This work was supported by grants from the National Key Research and Development Program of China (No. 2023YFB3208200), the equipment research and development projects of the Chinese Academy of Sciences (PTYQ2024YZ0010), the Science and Technology Commission of Shanghai Municipality Project (XTCX-KJ-2024-038), National Natural Science Foundation of China (62401555) and Shanghai Science and Technology Development Funds (23J21900100). This work was supported by the Postdoctoral Fellowship Program of CPSF under Grant Number GZC20232838.

Author details
[1]State Key Laboratory of Transducer Technology, Shanghai Institute of Microsystem and Information Technology, Chinese Academy of Sciences, Shanghai 200050, China. [2]School of Graduate Study, University of Chinese Academy of Sciences, Beijing 100049, China. [3]2020 X-Lab, Shanghai Institute of Microsystem and Information Technology, Chinese Academy of Sciences, Shanghai 200050, China. [4]School of Microelectronics, Shanghai University, Shanghai 200444, China. [5]Institute of Materiobiology, College of Science, Shanghai University, Shanghai 200444, China. [6]Shanghai Frontier Innovation Research Institute, Shanghai 201108, China

Conflict of interest
The authors declare no competing interests.

Supplementary information The online version contains supplementary material available at https://doi.org/10.1038/s41378-025-00914-6.

Received: 13 November 2024 Revised: 8 February 2025 Accepted: 24 February 2025
Published online: 12 May 2025

References

1. Whitesides, G. M. The origins and the future of microfluidics. *Nature* **442**, 368–373 (2006).
2. Dang, B. V. et al. Microfluidic actuation via 3D-printed molds toward multiplex biosensing of cell apoptosis. *ACS Sens.* **4**, 2181–2189 (2019).
3. Fair, R. B. Digital microfluidics: is a true lab-on-a-chip possible? *Microfluidics Nanofluidics* **3**, 245–281 (2007).
4. Frozanpoor, I., Cooke, M. D., Ambukan, V., Gallant, A. J. & Balocco, C. Continuous droplet-actuating platforms via an electric field gradient: Electrowetting and liquid dielectrophoresis. *Langmuir* **37**, 6414–6422 (2021).
5. Hartmann, J., Schür, M. T. & Hardt, S. Manipulation and control of droplets on surfaces in a homogeneous electric field. *Nat. Commun.* **13**, 289 (2022).
6. Geng, H., Feng, J., Stabryla, L. M. & Cho, S. K. Dielectrowetting manipulation for digital microfluidics: Creating, transporting, splitting, and merging of droplets. *Lab Chip* **17**, 1060–1068 (2017).
7. Wheeler, A. R. Putting electrowetting to work. *Science* **322**, 539–540 (2008).
8. Cheng, H., Liu, H. R., Li, W. H. & Li, M. Recent advances in magnetic digital microfluidic platforms. *Electrophoresis* **42**, 2329–2346 (2021).
9. Li, A. et al. Programmable droplet manipulation by a magnetic-actuated robot. *Sci. Adv.* **6**, eaay5808 (2020).
10. Huang, G. Y. et al. Magnetically actuated droplet manipulation and its potential biomedical applications. *Acs Appl. Mater. Interfaces* **9**, 1155–1166 (2017).
11. Rufo, J., Cai, F., Friend, J., Wiklund, M. & Huang, T. J. Acoustofluidics for biomedical applications. *Nat. Rev. Method Prim.* **2**, 30 (2022).
12. Wang, F. et al. Light control of droplets on photo-induced charged surfaces. *Natl Sci. Rev.* **10**, nwac164 (2023).
13. Xu, X. et al. Digital microfluidics for biological analysis and applications. *Lab Chip* **23**, 1169–1191 (2023).
14. Choi, K., Ng, A. H., Fobel, R. & Wheeler, A. R. Digital microfluidics. *Annu Rev. Anal. Chem.* **5**, 413–440 (2012).
15. Abdelgawad, M. & Wheeler, A. R. The digital revolution: a new paradigm for microfluidics. *Adv. Mater.* **21**, 920–925 (2009).
16. Kalsi, S. et al. Rapid and sensitive detection of antibiotic resistance on a programmable digital microfluidic platform. *Lab Chip* **15**, 3065–3075 (2015).
17. Zhang, Y. & Nguyen, N.-T. Magnetic digital microfluidics – a review. *Lab Chip* **17**, 994–1008 (2017).
18. Hu, X., Gao, X., Chen, S., Guo, J. & Zhang, Y. DropLab: an automated magnetic digital microfluidic platform for sample-to-answer point-of-care testing-development and application to quantitative immunodiagnostics. *Microsyst. Nanoeng.* **9**, 10 (2023).
19. Lin, H. S. et al. Ferrobotic swarms enable accessible and adaptable automated viral testing. *Nature* **611**, 570 (2022).
20. Huang, E. et al. Active droplet-array microfluidics-based chemiluminescence immunoassay for point-of-care detection of procalcitonin. *Biosens. Bioelectron.* **195**, 113684 (2021).
21. Zhang, J. et al. Wetting ridge assisted programmed magnetic actuation of droplets on ferrofluid-infused surface. *Nat. Commun.* **12**, 7136 (2021).
22. Lu, P. H., Ma, Y. D., Fu, C. Y. & Lee, G. B. A structure-free digital microfluidic platform for detection of influenza a virus by using magnetic beads and electromagnetic forces. *Lab Chip* **20**, 789–797 (2020).
23. Lehmann, U. et al. Two-dimensional magnetic manipulation of microdroplets on a chip as a platform for bioanalytical applications. *Sens. Actuat B: Chem.* **117**, 457–463 (2006).
24. Li, X. et al. Programmable digital liquid metal droplets in reconfigurable magnetic fields. *Acs Appl. Mater. Interfaces* **12**, 37670–37679 (2020).
25. Saroj, S. K., Asfer, M., Sunderka, A. & Panigrahi, P. K. Two-fluid mixing inside a sessile micro droplet using magnetic beads actuation. *Sens. Actuat A-Phys.* **244**, 112–120 (2016).
26. Seo, K., Wi, R., Im, S. & Kim, D. A superhydrophobic magnetic elastomer actuator for droplet motion control. *Polym. Advan. Technol.* **24**, 1075–1080 (2013).
27. Son, C. et al. Bidirectional Droplet Manipulation on Magnetically Actuated Superhydrophobic Ratchet Surfaces. *Acs Nano* **17**, 23702–23713 (2023).
28. Zeng, Y. et al. AIEgens-enhanced rapid sensitive immunofluorescent assay for SARS-CoV-2 with digital microfluidics. *Anal. Chim. Acta* **1298**, 342398 (2024).
29. Hu, S. et al. All-in-one digital microfluidics system for molecular diagnosis with loop-mediated isothermal amplification. *Biosensors* **12**, 324 (2022).
30. Li, S. et al. DECODE: contamination-free digital CRISPR platform for point-of-care detection of viral DNA/RNA. *ACS Sens.* **9**, 4256–4264 (2024).
31. Yang, B. et al. Automated study on kinetics and biosensing of glow-type luminescence reaction via digital microfluidics-chemiluminescence. *Lab chip* **23**, 785–792 (2023).
32. Rocha, D. S. et al. Digital microfluidic platform assembled into a home-made studio for sample preparation and colorimetric sensing of S-nitrosocysteine. *Anal. Chim. Acta* **1254**, 341077 (2023).
33. Kanitthamniyom, P. et al. A 3D-printed magnetic digital microfluidic diagnostic platform for rapid colorimetric sensing of carbapenemase-producing Enterobacteriaceae. *Microsyst. Nanoeng.* **7**, 47 (2021).
34. Sardini, E., Serpelloni, M. & Tonello, S. Printed electrochemical biosensors: Opportunities and metrological challenges. *Biosensors* **10**, 166 (2020).
35. Giménez-Gómez, P., Baldi, A., Ayora, C. & Fernández-Sánchez, C. Automated Determination of As(III) in Waters with an Electrochemical Sensor Integrated into a Modular Microfluidic System. *ACS Sens.* **4**, 3156–3165 (2019).
36. Rackus, D. G., Shamsi, M. H. & Wheeler, A. R. Electrochemistry, biosensors and microfluidics: a convergence of fields. *Chem. Soc. Rev.* **44**, 5320–5340 (2015).
37. Liao, Z. et al. Recent advances in microfluidic chip integrated electronic biosensors for multiplexed detection. *Biosens. Bioelectron.* **121**, 272–280 (2018).
38. Vinoth, R., Nakagawa, T., Mathiyarasu, J. & Mohan, A. M. V. Fully printed wearable microfluidic devices for high-throughput sweat sampling and multiplexed electrochemical analysis. *ACS Sens.* **6**, 1174–1186 (2021).
39. de Campos, R. P. S. et al. Plug-n-play" sensing with digital microfluidics. *Anal. Chem.* **91**, 2506–2515 (2019).
40. Long, Z., Shetty, A. M., Solomon, M. J. & Larson, R. G. Fundamentals of magnet-actuated droplet manipulation on an open hydrophobic surface. *Lab Chip* **9**, 1567–1575 (2009).
41. Malinowski, R., Parkin, I. P. & Volpe, G. Advances towards programmable droplet transport on solid surfaces and its applications. *Chem. Soc. Rev.* **49**, 7879–7892 (2020).
42. Wu, X. et al. Research progress of electrode shapes in EWOD-based digital microfluidics. *Rsc Adv.* **13**, 16815–16827 (2023).

43. Kremers, T., Thelen, S., Bosbach, N. & Schnakenberg, U. PortaDrop: A portable digital microfluidic platform providing versatile opportunities for Lab-On-A-Chip applications. *PLoS One* **15**, e0238581 (2020).
44. Zhang, Y. & Wang, T.-H. Full range magnetic manipulation of droplets via surface energy traps enables complex bioassays. *Adv. Mater.* **25**, 2903 (2013).
45. Jiang, S. et al. Sponge-inspired MXene@CeO2 detector for ultra-sensitive detection of glucose. *Mater. Today Chem.* **32**, 101638 (2023).
46. Fall, B. et al. Highly efficient non-enzymatic electrochemical glucose sensor based on carbon nanotubes functionalized by molybdenum disulfide and decorated with nickel nanoparticles (GCE/CNT/MoS2/NiNPs). *Sens. Actuat Rep.* **5**, 100136 (2023).
47. Wang, H. et al. An integrated nanoflower-like MoS2@CuCo2O4 heterostructure for boosting electrochemical glucose sensing in beverage. *Food Chem.* **396**, 133630 (2022).
48. Li, Q. F., Chen, X., Wang, H., Liu, M. & Peng, H. L. Pt/MXene-based flexible wearable non-enzymatic electrochemical sensor for continuous glucose detection in sweat. *ACS Appl Mater. Interfaces* **15**, 13290–13298 (2023).
49. Sharma, K. P., Shin, M., Awasthi, G. P., Cho, S. & Yu, C. One-step hydrothermal synthesis of CuS/MoS(2) composite for use as an electrochemical non-enzymatic glucose sensor. *Heliyon* **10**, e23721 (2024).
50. Wang, J. et al. Preparation of MoS2@AuNP nanocomposite by a self-reduction method and its application for electrochemical glucose sensing. *Mater. Adv.* **3**, 8677–8683 (2022).